Research Article

NMR IN BIOMEDICINE

Received: 10 February 2010, Revised: 2 June 2010, Accepted: 3 June 2010, Published online in Wiley Online Library: 27 August 2010

(wileyonlinelibrary.com) DOI:10.1002/nbm.1585

Real-time MRI at a resolution of 20 ms

Martin Uecker[a], Shuo Zhang[a], Dirk Voit[a], Alexander Karaus[a], Klaus-Dietmar Merboldt[a] and Jens Frahm[a]*

The desire to visualize noninvasively physiological processes at high temporal resolution has been a driving force for the development of MRI since its inception in 1973. In this article, we describe a unique method for real-time MRI that reduces image acquisition times to only 20 ms. Although approaching the ultimate limit of MRI technology, the method yields high image quality in terms of spatial resolution, signal-to-noise ratio and the absence of artifacts. As proposed previously, a fast low-angle shot (FLASH) gradient-echo MRI technique (which allows for rapid and continuous image acquisitions) is combined with a radial encoding scheme (which offers motion robustness and moderate tolerance to data undersampling) and, most importantly, an iterative image reconstruction by regularized nonlinear inversion (which exploits the advantages of parallel imaging with multiple receiver coils). In this article, the extension of regularization and filtering to the temporal domain exploits consistencies in successive data acquisitions and thereby enhances the degree of radial undersampling in a hitherto unexpected manner by one order of magnitude. The results obtained for turbulent flow, human speech production and human heart function demonstrate considerable potential for real-time MRI studies of dynamic processes in a wide range of scientific and clinical settings. Copyright © 2010 John Wiley & Sons, Ltd.

Supporting information may be found in the online version of this article.

Keywords: dynamic imaging; MRI; real time; movie; turbulent flow; speech production; heart function; cardiovascular MRI

INTRODUCTION

Since the conception of MRI by Lauterbur (1), a major driving force for its further technical, scientific and clinical development has been the quest for speed. Historically, it took more than a decade before the fast low-angle shot (FLASH) MRI technique (2) reduced the acquisition times for a cross-sectional image to the order of 1 s, and allowed us to perform continuous imaging as a result of the generation of a sufficiently strong steady-state MRI signal. Nevertheless, the monitoring of dynamic processes in real time (3) remains hampered for two reasons: the need for relatively long measurement times of several hundreds of milliseconds for images with a reasonable spatial resolution, and the use of Cartesian encoding schemes that sample the MRI data space (*k* space) on a rectilinear grid.

Cartesian sampling refers to the acquisition of parallel lines in *k* space, and was preferred because of its tolerance to the instrumental imperfections of early MRI systems and the simple reconstruction of an image by inverse fast Fourier transformation (FFT) of the raw data. Despite these advantages for static images, the continuous monitoring of a moving object is better served with radial encoding schemes, as the information content of an individual 'spoke' in *k* space is of equal importance for the reconstructed image. This is because each spoke, but not each parallel line, crosses the center of *k* space and therefore contributes both high spatial frequencies (outer parts of *k* space) and low spatial frequencies (central *k* space). Only the latter determine the gross image content, such as the position of a moving object.

On the other hand, the use of high-speed acquisition techniques for real-time MRI suffers from a number of specific drawbacks. For example, so-called single-shot gradient-echo sequences, such as echo-planar imaging (4–6) and spiral imaging (7,8), are prone to geometric distortions or even local signal losses that are caused by their inherent sensitivity to off-resonance effects, tissue susceptibility differences and magnetic field inhomogeneities, which are unavoidable in many parts of the body. Complementary, single-shot MRI sequences that employ radiofrequency (RF)-refocused spin echoes (9) or stimulated echoes (10), and therefore are free from such problems, lead to a pronounced RF power absorption with the risk of local tissue heating, or suffer from a compromised signal-to-noise ratio (SNR), respectively.

Backed by the observation that radial encoding schemes may resolve some of the earlier problems of dynamic Cartesian imaging (11), we have recently described a real-time MRI method based on a radially encoded FLASH MRI sequence (12). However, image reconstruction was performed by gridding, which is a rectilinear interpolation of *k* space in combination with a density compensation and inverse FFT. With this method, rates of up to 20 frames per second are only obtainable when using a sliding window or fluoroscopy (13) approach, and the true temporal fidelity of the images is still determined by measurement times

* *Correspondence to: J. Frahm, Biomedizinische NMR Forschungs GmbH am Max-Planck-Institut für biophysikalische Chemie, 37070 Göttingen, Germany. E-mail: jfrahm@gwdg.de*

a *M. Uecker, S. Zhang, D. Voit, A. Karaus, K.-D. Merboldt, J. Frahm Biomedizinische NMR Forschungs GmbH am Max-Planck-Institut für biophysikalische Chemie, Göttingen, Germany*

Abbreviations used: *FFT, fast Fourier transform; FLASH, fast low-angle shot; FOV, field of view; GPU, graphical processing unit; RF, radiofrequency; SNR, signal-to-noise ratio.*

of 200–250 ms. For TR = 2 ms, these durations correspond to the necessary acquisition of 100–125 radial spokes for an image with a base resolution of 128 data points per spoke and a 128×128 image matrix.

In this article, we present a novel solution which reduces the minimum imaging time for real-time MRI by another order of magnitude. The proposed method combines radial FLASH MRI (12) with image reconstructions by regularized nonlinear inversion, which we originally developed for improved parallel MRI using Cartesian encodings (14). More recently, the algorithm was adopted to radial trajectories and modified for parallelization and implementation on graphical processing units (GPUs) (15). In the present work, we further refined the reconstruction process by extending the regularization and filtering to the temporal domain in order to exploit temporal consistencies in successive data acquisitions. The resulting method allows for an unexpected degree of data undersampling and correspondingly short image acquisition times. For example, for a 128×128 matrix, it is possible to reconstruct each image in a time series from only nine spokes, which may be acquired within a total imaging time of 18 ms. Because a fully sampled acquisition would require $\pi/2 \times 128 = 205$ spokes, these conditions correspond to undersampling factors of about 20, which cause a complete failure of gridding reconstructions (12,16).

METHODS

Subjects

Human participants with no known illnesses were recruited among the students of the local university and received a reimbursement of 10 Euros/h. For studies of speech production and cardiac function, we used a total of eight and 12 subjects, respectively. Four subjects were studied on several occasions to assess intra-individual reproducibility. For MRI, subjects were examined in a supine position in all cases. All subjects gave written informed consent before each MRI examination.

Radial FLASH MRI

All MRI studies were conducted at 3 T using an unmodified commercially available MRI system (Tim Trio, Siemens Healthcare, Erlangen, Germany) and a body coil for RF excitation. Magnetic field gradients were applied in 'normal' mode rather than with the fastest possible switching times to avoid peripheral nerve stimulation in human studies under all circumstances (e.g. for double oblique section orientations in cardiac real-time MRI at high frame rates).

We used an RF-spoiled FLASH MRI sequence for data acquisition (Fig. 1a) yielding spin density or T_1 contrast depending on TR and the flip angle of the RF excitation pulse. The implementation employed a strongly undersampled radial encoding scheme with an interleaved multi-turn arrangement for five successive images (Fig. 1b). Each single turn corresponds to a full image and contains only a small number of spokes (typically 9–25) that are equally distributed over a full 360°circle in order to homogeneously sample the *k* space. The chronological order of the acquired spokes was chosen to be sequential within each turn.

The interleaved strategy has several advantages. First, residual streaking artifacts caused by reconstructions from very small datasets will differ from frame to frame and may be removed by mild temporal filtering. Second, interleaved schemes offer the possibility for retrospective reconstructions with different spatiotemporal resolutions by combining successive single-turn acquisitions. Third, because most current MRI systems do not yet have sufficient computing power for iterative real-time

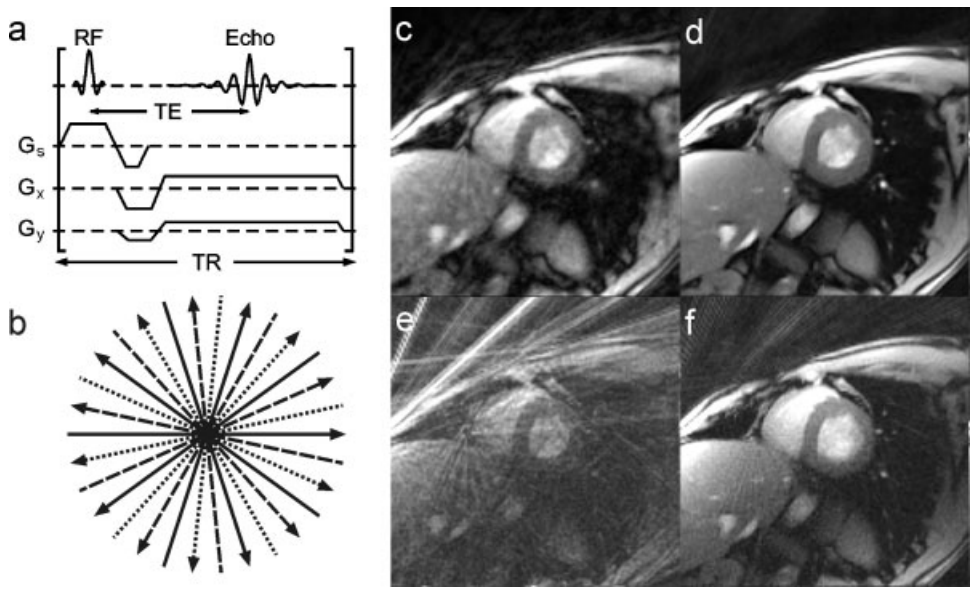

Figure 1. Real-time MRI. (a) Generic fast low-angle shot (FLASH) MRI sequence with radial data encoding: Echo, gradient echo; Gs, slice-selective gradient; Gx, Gy, encoding gradients; RF, radiofrequency excitation pulse; TE, echo time; TR, repetition time. (b) The radial encoding scheme covers the data space with spokes that are homogeneously distributed over 360°, and successive frames employ interleaved arrangements. The example refers to three sequential image acquisitions (full, broken and dotted lines) with five spokes each. Arrows indicate readout directions. (c) Nonlinear inverse reconstruction of a post-systolic frame from a real-time MRI movie of the human heart according to ref. (15), without temporal regularization and filtering (in-plane resolution, 2.0 mm; section thickness, 8 mm; TR = 2.0 ms; 15 spokes; imaging time, 30 ms). (d) Same as (c) but with temporal regularization and temporal median filtering. (e) Gridding reconstruction of the same data as in (c). (f) Gridding reconstruction of a dataset comprising 75 spokes (imaging time, 150 ms) that centrally covers the data used for reconstructions (c)–(e). For details, see text.

reconstructions, multi-turn datasets may also be used for online sliding window reconstructions based on gridding. Indeed, although nonlinear inverse reconstructions were obtained from each single turn (see below), online control of real-time acquisitions was accomplished with the use of less undersampled datasets (12) by combining data from five consecutive turns and reconstructing respective images by gridding (17–19) with a sliding window (13).

Nonlinear inverse reconstruction

Reconstructions using regularized nonlinear inversion were performed offline for single-turn radial encodings with 9–25 spokes. Corresponding movies consisted of successive reconstructions without a sliding window, but with the use of a temporal filter to remove residual reconstruction artifacts (see below). We therefore achieved frame rates that correspond to the reciprocal of the actual image acquisition time. All radial spokes were acquired with oversampling by a factor of two, so that a base resolution of 128 data samples per spoke resulted in 256 complex samples for image reconstruction. The procedure ensures the absence of image aliasing for fields of view smaller than the actual object.

The basic algorithm for image reconstruction by regularized nonlinear inversion has been described previously (14,15). A comprehensive mathematical formulation of the extended reconstruction process used here is summarized in the Appendix. Briefly, parallel MRI reconstructions (20,21) may be improved significantly if image content and coil sensitivities are jointly estimated from the entire available data (14). As a consequence, the MRI signal equation becomes a nonlinear equation, which may be solved with numerical methods, such as the iteratively regularized Gauss–Newton method (22). Because the reconstruction requires an initial estimate, the image is initialized to unity and the coil sensitivities to zero, although, for a time series, this may be replaced by the previous frame. The regularization term strongly penalizes high spatial frequencies in the coil sensitivities, whilst using a conventional L^2 regularization for the image. For the reconstruction of serial images as accomplished here, the algorithm was further modified to include a temporal regularization with respect to the previous frame.

The reconstruction by nonlinear inversion was recently adapted to non-Cartesian trajectories (15) by a technique similar to convolution-based sensitivity encoding (23). This technique moves the interpolation into a single preceding processing step, and all iterative computations are performed on the Cartesian grid. This modification facilitates the parallelization and implementation of the algorithm on GPUs, which may be exploited to realize considerable reductions in the reconstruction time (15). In this work, four Tesla C1060 GPUs (Nvidia, Santa Clara, CA, USA) were used, each providing 240 processing cores. Typically, the iterative reconstruction of a single frame with a final 128×128 image matrix took about 2.5 s per GPU.

For all examples shown here, the following preprocessing steps were performed. To reduce the computation time, the raw data from all (up to 32) receiver channels were reduced to 12 principal components by a channel compression technique (12,24). The reduced data were then interpolated to the processing grid and normalized such that the L^2 norm after interpolation to the processing matrix was 100. The data were then transferred to the GPU for reconstruction. Further details on specific reconstruction parameters are given in Table 1.

After completion of the reconstruction process, consecutive frames of a movie were temporally filtered using a median filter (25) extending over five images. This value has been chosen to correspond to the interleaved spoke arrangement: it effectively reduces residual reconstruction (streaking) artifacts that differ from frame to frame according to the angular displacement of the acquired spokes. Accordingly, the image intensities of each frame are replaced by the median of five frames, including the two preceding and following frames. In principle, similar results may be achieved with the use of a three-turn spoke arrangement in conjunction with a median filter extending over three images (data not shown). Indeed, if only very small or no residual reconstruction artifacts are to be removed, the best temporal fidelity may be achieved by reconstructions without any temporal filter. As a final processing step, the images were subjected to spatial filtering, which involves a medium edge enhancement and adaptive smoothing, taking into account the continuation of local tissue structures (in part using software supplied by Siemens Healthcare).

Table 1. Acquisition and processing parameters for real-time MRI

	Flow (Fig. 4)	Speech (Fig. 5)	Heart (Fig. 6)
Imaging time (ms)	20	55	30
Rate (frames/s)	50	18	33
Resolution (mm^3)	$1.5 \times 1.5 \times 8$	$1.5 \times 1.5 \times 10$	$2.0 \times 2.0 \times 8$
Field of view (mm^2)	256×256	192×192	256×256
Reconstruction matrix	176×176	128×128	128×128
Acquired spokes	9	25	15
TR (ms)	2.2	2.2	2.0
TE (ms)	1.4	1.4	1.3
Flip angle (deg)	8	5	8
Bandwidth (Hz/pixel)	1580	1630	1955
Processing matrix[a]	352×352	384×384	384×384
Newton steps[a]	7	9	7
Scale factor for regularization[a]	0.8	1.0	1.0

[a]See Appendix.

Real-time MRI studies

The development of turbulent flow patterns in a cylindrical beaker (inner diameter, 144 mm) filled with tap water (height about 30 mm) was observed for 60 s after manual stirring for about 5 s. The beaker was positioned within a standard 32-channel head coil. The horizontal images at medium height covered a 256×256-mm^2 field of view (FOV) with a base resolution of 176 data samples (1.5×1.5 mm^2; section thickness, 8 mm). RF-spoiled FLASH MRI acquisitions employed TR = 2.2 ms, gradient TE = 1.4 ms and a flip angle of 8°, yielding T_1 contrast. Movies were acquired with different frame rates, although the best results were obtained for 50 frames per second, corresponding to image acquisition times of 20 ms (nine spokes). Further details are given in Table 1.

Studies of human speech production were performed in a mid-sagittal orientation covering the lips, tongue, soft palate, pharyngeal area and vocal fold. The acquisitions combined the posterior 16-coil array of the 32-channel head coil with a surface coil (diameter, 70 mm) next to the larynx and a flexible four-array coil positioned in a circular shape over the lower face at a distance of about 20 mm. Preliminary applications focused on the co-articulation of vowels (e.g. [a], [u], [i]) and plosives (e.g. [t], [d]) in simple German logatoms, such as [butu] or [bidi]. RF-spoiled FLASH MRI acquisitions (1.5×1.5 mm^2; section thickness, 10 mm) employed TR = 2.2 ms, gradient TE = 1.4 ms (opposed-phase condition for overlapping proton signals from water and fat at 3 T) and a flip angle of 5°. The images covered a 192×192-mm^2 FOV with a matrix of 128×128 data samples. Real-time movies were obtained at 18–30 frames per second, corresponding to image acquisition times of 33–55 ms (15–25 spokes). For the present examples of speech production at moderate speed, best results were achieved for 25 spokes at 18 frames per second. Further details are given in Table 1.

Real-time MRI of the human heart without synchronization to the electrocardiogram and during free breathing was performed with a 32-channel cardiac coil consisting of an anterior and posterior 16-coil array. T_1-weighted RF-spoiled FLASH MRI acquisitions (2.0×2.0 mm^2; section thickness, 8 mm) employed TR = 2.0 ms, gradient TE = 1.3 ms (opposed-phase condition) and a flip angle of 8°. The images covered a 256×256-mm^2 FOV with a base resolution of 128 data samples. As in the aforementioned applications, movies were obtained for a wide range of rates from 20 to 55 frames per second with corresponding imaging times of 50 to 18 ms (25 to nine spokes). Recordings in different anatomically defined orientations included short-axis views, two-chamber views and four-chamber views covering the entire heart in sequential scans. Further details are given in Table 1.

RESULTS

The performance of the proposed reconstruction process is demonstrated in Fig. 1c–f for the case of a post-systolic heart image obtained in 30 ms (15 spokes, TR = 2.0 ms). A comparison of the frame reconstructed according to the method described in ref. (15), that is without temporal regularization and filtering (Fig. 1c), with a reconstruction as proposed here (Fig. 1d) reveals no loss in temporal acuity for the latter image, but an enhanced sharpness and a reduction in residual streaking artifacts. A reconstruction of the same frame by gridding (Fig. 1e) is unable to yield reasonable image quality. Moreover, a gridding reconstruction (Fig. 1f) of a five times longer acquisition (75 spokes, 150 ms), which includes the same time period as used for the nonlinear inverse reconstructions shown in Fig. 1c, d, demonstrates pronounced temporal blurring of the myocardial wall during the rapid post-systolic expansion of the heart.

The improved performance of the proposed method is further detailed by a series of five consecutive frames (15 spokes, 30 ms) shown in Fig. 2, which characterize the same post-systolic expansion phase of the myocardium as shown in Fig. 1. The comparison of the reconstructions according to ref. (15) (Fig. 2a) with reconstructions including a temporal regularization (Fig. 2b) reveals a clearly enhanced sharpness of the images that arises from the incorporation of temporal constraints. The addition of a temporal median filter (Fig. 2c) does not impair this sharpness, but mainly removes residual streaking artifacts that change from frame to frame because of the interleaved encoding scheme. The final use of mild spatial filtering (Fig. 2d) reduces the noise without contributing visible blurring.

Figure 3 shows the achievable image quality for the proposed nonlinear inverse reconstruction method as a function of temporal resolution (or degree of undersampling). These diastolic and systolic short-axis views of the human heart were selected from respective real-time MRI movies. The images were obtained from only 25, 15 and nine spokes (128×128 matrix) with acquisition times of 50, 30 and 18 ms, respectively.

The possibility to analyze noninvasively dynamic processes by real-time MRI lends itself to a wide range of promising applications in the natural sciences and medicine. The visualization of turbulent flow in a beaker of water after manual stirring serves as a simple demonstration for this capacity. A comparison of the flow dynamics in the selected 200-ms periods at 10 s (Fig. 4a) and 30 s after the end of stirring (Fig. 4b) indicates a mean velocity decrease by about one order of magnitude from about 0.1 to 0.01 m/s, as estimated from the coherent movement of MRI signal patterns with reference to the known dimensions of the image. The T_1-weighted images have a temporal resolution of 20 ms (nine spokes, TR = 2.2 ms) and result in movies with a rate of 50 frames per second (Video S1, see Supporting Information). In the absence of a contrast agent, their native T_1 contrast unravels flow components perpendicular to the imaging plane. Because the magnetizations of slow or stationary water protons within the plane become partially saturated by experiencing many successive RF excitations, they appear darker than the signals from water protons, which freshly enter the excited plane from neighboring locations without RF excitation, and therefore contribute an unsaturated (bright) spin-density signal without T_1 weighting. Indeed, when comparing movies with different frame rates (imaging times), the fastest acquisitions are favorable with respect to temporal acuity (lack of temporal blurring) and SNR. This observation seems to be because most of the signal (and contrast) results from the inflow of unsaturated water protons crossing the imaging plane.

Another example is the investigation of human speech production, which is of linguistic interest but may also have clinical relevance. We performed a preliminary phonetic study of the co-articulation of vowels (e.g. [a], [u], [i]) and plosives (e.g. [t], [d]) in German logatoms, such as [butu], in a mid-sagittal orientation covering the entire articulation organs, including the lips, tongue, soft palate, pharyngeal area and vocal fold (Fig. 5). The selected 660-ms period centers on the articulation of the plosive [t] between the two vowels [u]. With speech production at moderate speed, this event is characterized by an elevation of the

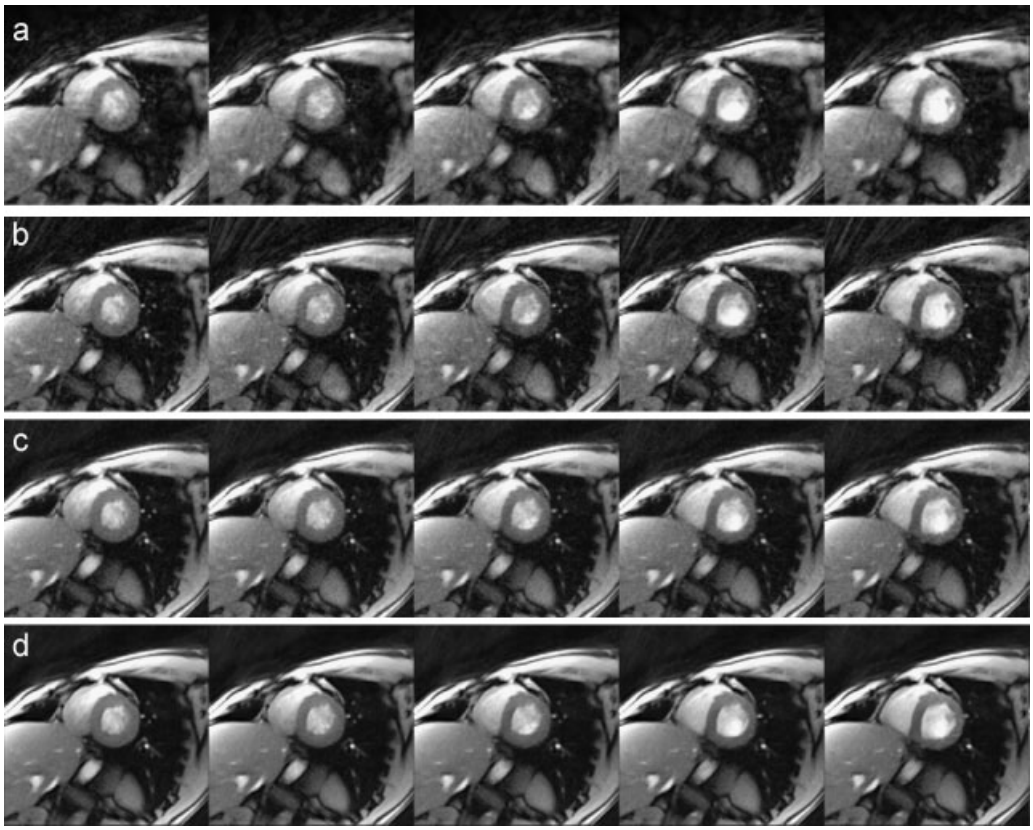

Figure 2. Nonlinear inverse reconstructions of five consecutive post-systolic frames from a real-time MRI movie of the human heart (same data as in Fig. 1). (a) Reconstructions according to ref. (15) without temporal regularization and filtering; (b) with temporal regularization; (c) with additional temporal median filtering; (e) with additional spatial filtering.

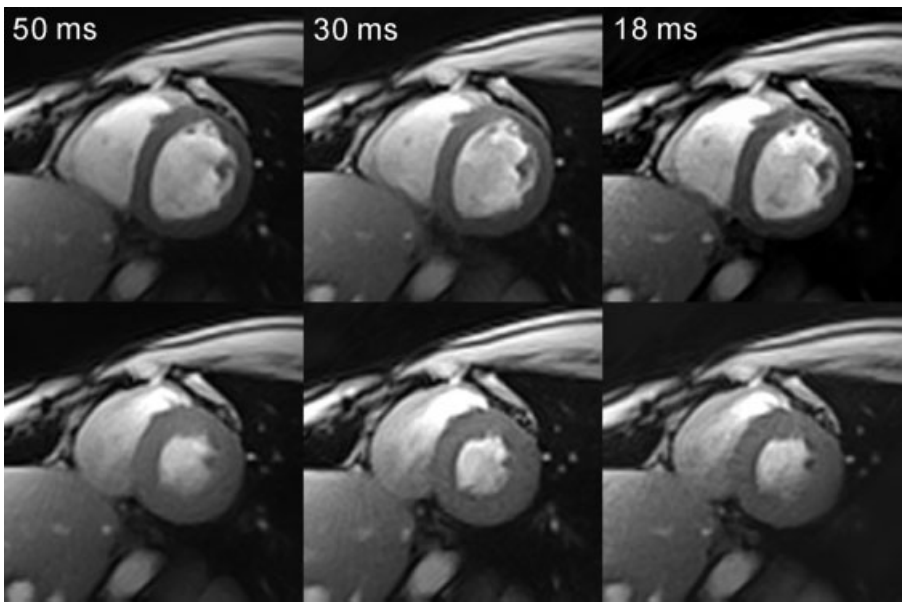

Figure 3. Real-time MRI reconstructions as a function of acquisition time or degree of undersampling. Nonlinear inverse reconstructions with temporal and spatial filtering of diastolic (top) and systolic (bottom) frames from real-time MRI movies of the human heart (in-plane resolution, 2.0 mm; section thickness, 8 mm; TR = 2.0 ms) acquired from only 25 spokes (imaging time, 50 ms), 15 spokes (30 ms) and nine spokes (18 ms). The nonlinear inverse algorithm allows for a reconstruction with an undersampling factor of 20, as a fully sampled image with a 128×128 matrix would require 205 spokes.

NMR IN BIOMEDICINE

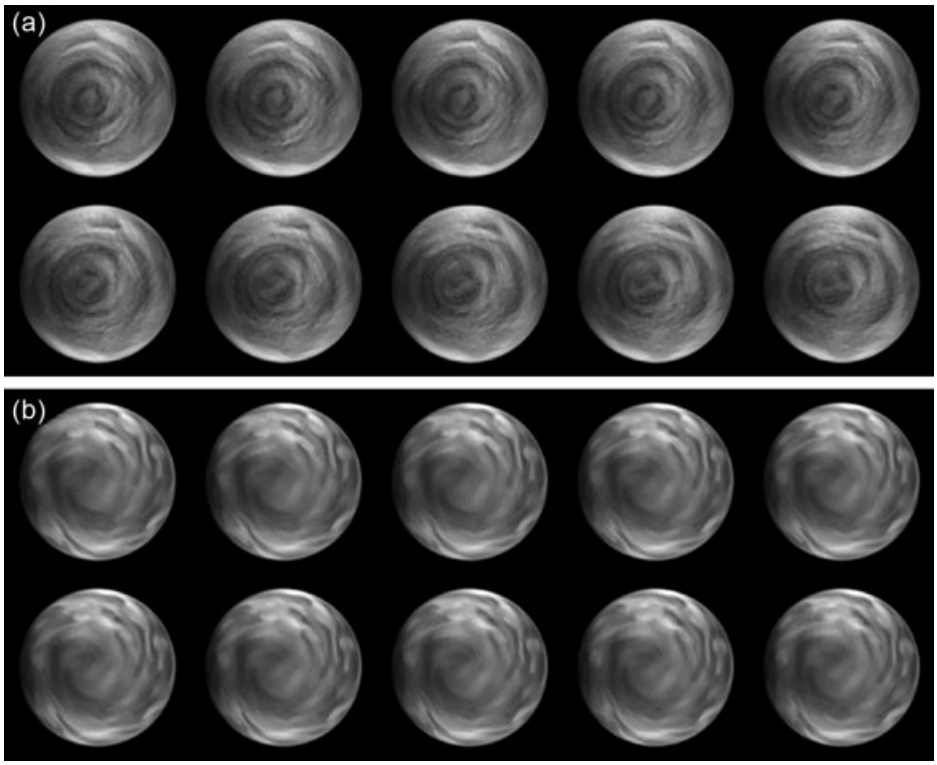

Figure 4. Real-time MRI of turbulent flow at a resolution of 20 ms. The two sets of T_1-weighted images (10 successive frames = 200 ms, top left to bottom right) refer to a horizontal section through a circular beaker filled with tap water. They were selected from the same movie at about 10 s (a) and 30 s (b) after the end of manual stirring, and reflect flow patterns with different velocities. Individual images (in-plane resolution, 1.5 mm; section thickness, 8 mm) were acquired within 20 ms (nine spokes, TR = 2.2 ms), corresponding to a rate of 50 frames per second.

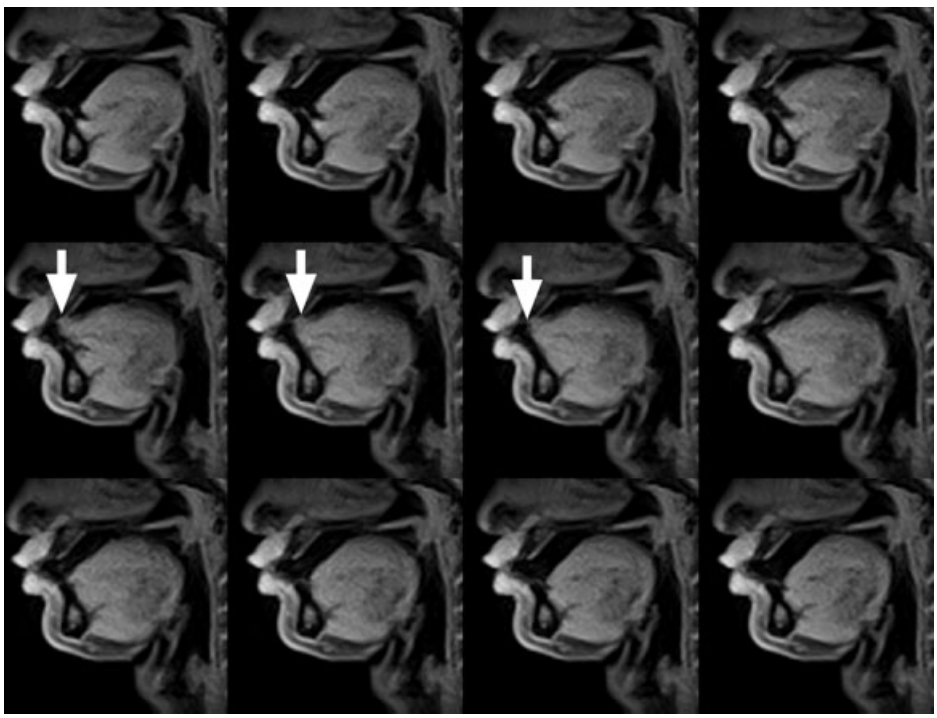

Figure 5. Real-time MRI of speech production at a resolution of 55 ms. The images (12 successive frames = 660 ms, top left to bottom right) were obtained from a healthy subject during speaking of the German logatom [butu]. The selected period centers on the articulation of the plosive [t] (arrows) with the tongue touching the upper alveolar ridge for about 150 ms. Individual images (mid-sagittal orientation; in-plane resolution, 1.5 mm; section thickness, 10 mm) were acquired within 55 ms (25 spokes, TR = 2.2 ms), corresponding to a rate of 18 frames per second.

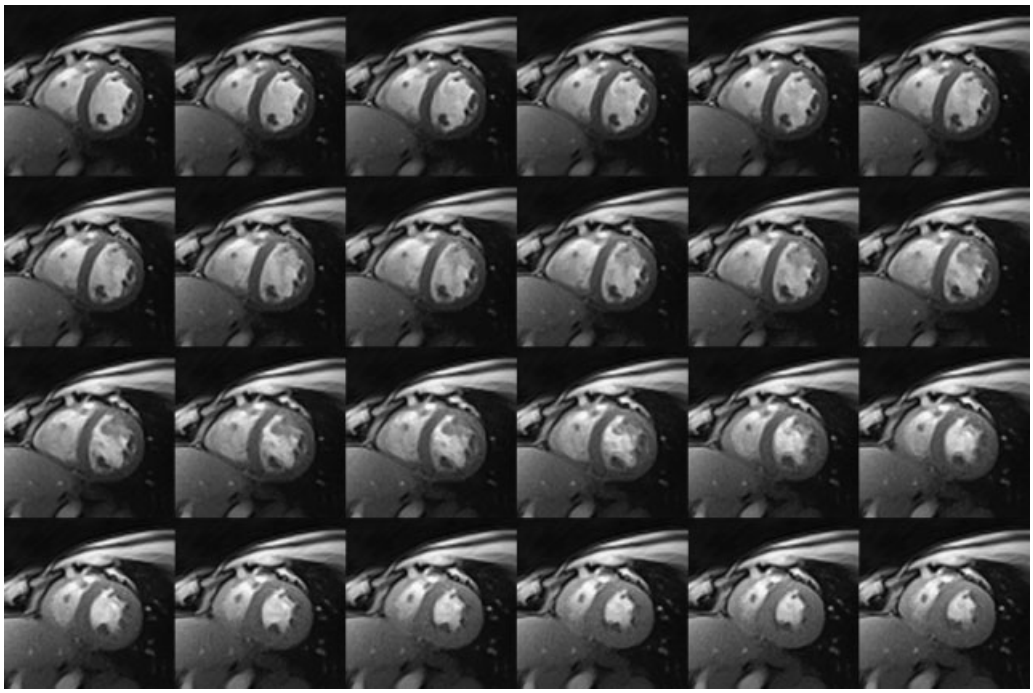

Figure 6. Real-time MRI of the human heart at a resolution of 30 ms. The short-axis views (24 successive frames = 720 ms) were obtained from a healthy subject during free breathing, and extend over about three-quarters of a cardiac cycle from diastole (top left) to systole (lower right). Individual images (in-plane resolution, 2.0 mm; section thickness, 8 mm) were acquired within 30 ms (15 spokes, TR = 2.0 ms), corresponding to a rate of 33 frames per second.

soft palate, contraction and release of the vocal fold, a fast movement of the tongue and a brief touching of the upper alveolar ridge for about 150 ms. Accordingly, when comparing real-time MRI acquisitions at different frame rates, best results in terms of temporal accuracy and SNR were obtained for movie acquisition at 18 frames per second (Video S2, see Supporting Information), which corresponds to image acquisition times of 55 ms (TR = 2.2 ms, 25 spokes).

One of the most relevant clinical applications of real-time MRI is, of course, cardiovascular imaging (Fig. 6). This is because examinations of myocardial anatomy and function without the need for synchronization with the electrocardiogram, and during free breathing, are not only beneficial to patients, but are also expected to improve the diagnostic quality of the examination by eliminating both motion artifacts and temporal blurring in cine reconstructions from multiple (and, in many pathological cases, irregular) heart beats. In this first assessment of the technique in healthy subjects, we found that a rate of 33 frames per second provided an adequate solution in terms of spatial resolution (2 mm) and temporal resolution with imaging times of 30 ms (TR = 2.0 ms, 15 spokes). The selected period depicts about three-quarters of a single cardiac cycle from diastole to systole (contraction and thickening of the myocardial wall) in an anatomically defined short-axis view selected from a corresponding real-time MRI movie (Video S3, see Supporting Information).

DISCUSSION

Our solution to real-time MRI offers pronounced motion robustness, high image quality and a flexible temporal resolution, spatial resolution and image contrast without suffering from sensitivities to off-resonance artifacts or restrictions caused by RF power deposition. The key to this achievement is the combination of a radial FLASH MRI acquisition with an image reconstruction by regularized nonlinear inversion, which leads to a hitherto unexpected potential to reduce the number of spokes per image. Indeed, the method combines several advantages: continuous updating of the coil sensitivities for all time frames; implicit data reduction capacity of parallel MRI acquisitions; tolerance of radial encodings to undersampling; enhanced tolerance of the nonlinear algorithm to undersampling; temporal regularization; and temporal filtering in conjunction with an interleaved encoding scheme for sequential frames. Taken together, the proposed method improves the temporal resolution of MRI by one order of magnitude in comparison with preceding gridding reconstructions.

In comparison with MRI reconstructions based on compressed sensing (26), the current approach does not require sparsity, and therefore reduces the complexity of the minimization problem. Moreover, the algorithm is free from model assumptions, as employed, for example, for highly accelerated time-resolved MR angiograms (27). In a similar manner, the proposed method does not depend on the specific nature of the *k*–*t* space, as required, for example, for UNFOLD (unaliasing by Fourier-encoding the overlaps using the temporal dimension) (28) and TSENSE (adaptive sensitivity encoding incorporating temporal filtering) (29).

Further technical progress is to be expected. In particular, this applies to more efficient modifications of the algorithm for parallelized GPU implementations as a prerequisite for immediate online reconstructions. Other aspects refer to the replacement of the temporal filter by integrating more sophisticated criteria of spatiotemporal consistency into the reconstruction algorithm, as well as an automated and locally adaptive optimization of the regularization parameter.

The real-time MRI technology described here will find many new applications in different areas of research. For example,

nonmedical applications may address the hydrodynamic properties of mixed fluids in a variety of physicochemical systems and, in particular, focus on the three-dimensional characterization of turbulent flow phenomena. Moreover, the widespread availability of clinical MRI systems will lead to a pronounced influence on biomedical and clinical imaging scenarios. This is further supported by the ease of implementation of the acquisition technique and the expected refinement of the existing computer hardware for speeding up iterative reconstructions. Immediate impact is to be expected on cardiovascular MRI, because of the ability to assess myocardial functions in real time with high temporal resolution. Indeed, preliminary results indicate the potential to monitor the functioning of cardiac valves and to determine the properties of (turbulent) blood flow in the heart and large vessels. Moreover, based on the insensitivity of the proposed method to susceptibility-induced image artifacts, we foresee a renewed interest in interventional MRI, which refers to the real-time monitoring of minimally invasive surgical procedures.

The real-time MRI method presented here also offers other possibilities, such as the dynamic assessment of joint movements and the online visualization of rapid physiological processes, for example after the administration of an MRI contrast agent. Indeed, if specific applications do not require maximum temporal resolution, the use of a lower frame rate may be translated into better spatial resolution or the simultaneous recording of movies in multiple sections. Alternatively, real-time MRI may be combined with the encoding of additional information, for example on flow velocities, using phase contrast techniques. In summary, the proposed method enhances the potential of MRI in a wide range of applications.

APPENDIX: COMPREHENSIVE ALGORITHM FOR RECONSTRUCTIONS BY REGULARIZED NONLINEAR INVERSION

Autocalibrated parallel imaging as a nonlinear inverse problem

The MRI signal equation for an image ρ with S RF coils and respective sensitivities c_j is given by:

$$y_j(t) = \int_{\Omega} d\vec{x}\, \rho(\vec{x})\, c_j(\vec{x})\, e^{-i\vec{k}(t)\vec{x}} \qquad [1]$$

where $\vec{k}$ refers to the k space trajectory and y_j to the signal received in channel j. The signal equation can be understood as an ill-conditioned nonlinear inverse problem $F\,x = y$. The operator F maps the unknown image ρ represented as an element of L^2 space over an area Ω containing the FOV and the S sensitivities c_j, which are smooth functions in a Sobolev space H^l of order $l = 16$, to the acquired k space positions:

$$\begin{aligned} F : L^2(\Omega, \mathbf{C}) \times H^l(\Omega, \mathbf{C}^S) &\rightarrow L^2\left(range\left(\vec{k}\right), \mathbf{C}^S\right) \\ (\rho, c_j) &\rightarrow y_j = \int_{\Omega} d\vec{x}\, \rho(\vec{x})\, c_j(\vec{x})\, e^{-i\vec{k}(t)\vec{x}} \end{aligned} \qquad [2]$$

Discretization

After discretization on a rectangular Cartesian grid, the operator F can be decomposed into five operators $F = P_k$ DTFT M_Ω C W^{-1}, where P_k is the projection onto the measured sample positions, DTFT is the multidimensional discrete time (here space) Fourier transform and M_Ω is a mask which restricts the reconstructed image to the area Ω. The only nonlinear operation is performed by operator C which multiplies image and coil sensitivities. The matrix W is a weighted discrete Fourier transform, which acts only on the sensitivity components of x but not on the image. W causes a Fourier weighting of the form $(1 + 225|k|^2)^{16}$ (with $-0.5 < k_x, k_y < 0.5$), and is used to embed the discretized Sobolev space of the coil sensitivities into some finite complex vector space with the standard scalar product.

Regularized nonlinear inversion

Image content and coil sensitivities are jointly estimated by solving the equation $F\,x = y$ using N steps of the iteratively regularized Gauss–Newton method (22). Starting from an initial estimate x_0, each iteration step consists of solving a regularized linearization

$$\begin{aligned} &\left(\mathrm{DF}_{x_n}^{\mathrm{H}}\,\mathrm{DF}_{x_n} + \alpha_n I\right)(x_{n+1} - x_n) \\ &\quad = \mathrm{DF}_{x_n}^{\mathrm{H}}(y - Fx_n) - \alpha_n(x_n - x_{\mathrm{ref}}) \end{aligned} \qquad [3]$$

of the equation $F\,x = y$ at the current estimate x_n for the next estimate x_{n+1} with the use of the conjugate gradient algorithm. Here, DF is the Fréchet derivative of F at x_n and DF^{H} is its adjoint.

Prior to the iteration, the data y is normalized to 100 in the L^2 norm. Image components of x_0 are set to unity and coil components of x_0 are set to zero for the first frame of a series, whereas, for later frames, the final estimate $x^{\mathrm{prev}}{}_N$ of the preceding frame is used as the initial estimate.

For the reconstruction of serial image acquisitions, the algorithm may be extended by a temporal regularization with respect to the previous frame. In this case, the regularization term is complemented by a reference x_{ref} for the image and coil sensitivities. Although using zero for the first frame, the reference x_{ref} for the following frames is set to the final estimates $x^{\mathrm{prev}}{}_N$ of the image and sensitivities of the previous frame with the optional application of a scaling factor. The regularization parameter α_n is reduced in each Newton step according *to* $\alpha_n = 2^{-n}$. Accordingly, the effective regularization of the reconstructed image is the regularization used in the last iteration, and is therefore controlled by the total number of Newton steps.

Implementation for non-Cartesian (radial) data

Inserting the operator F into the update rule of the iteratively regularized Gauss–Newton method yields two terms which are not straightforward to implement for non-Cartesian data. Although the operator M_Ω DTFT^{-1} P_k DTFT M_Ω must be applied during each iteration of the conjugate gradient algorithm, the term M_Ω DTFT^{-1} y only needs to be evaluated once for each image as a preprocessing step. The first term can be understood as a convolution with the point-spread function restricted to a certain area defined by the mask M_Ω, which is implemented with two applications of a FFT algorithm on an increased processing matrix. The second term, M_Ω DTFT^{-1} y, is the adjoint of a nonequidistant Fourier transform, which is implemented by interpolating the data y onto a two-fold oversampled Cartesian grid with the use of a Kaiser–Bessel window ($L = 6$, $\beta = 13.8551$), followed by a roll-off correction.

REFERENCES

1. Lauterbur PC. Image formation by induced local interactions: examples employing nuclear magnetic resonance. Nature, 1973; 242: 190–191.
2. Frahm J, Haase A, Matthaei D, Hänicke W, Merboldt KD. German Patent P 3504734.8, 12 February 1985.
3. Frahm J, Haase A, Matthaei D. Rapid NMR imaging of dynamic processes using the FLASH technique. Magn. Reson. Med. 1986; 3: 321–327.
4. Mansfield P, Pykett IL. Biological and medical imaging by NMR. J. Magn. Reson. 1978; 29: 355–373.
5. Ordidge RJ, Mansfield P, Doyle M, Coupland RE. Real time movie images by NMR. Br. J. Radiol. 1982; 55: 729–733.
6. Mansfield P. Real-time echo-planar imaging by NMR. Br. Med. Bull. 1984; 40: 187–190.
7. Ahn CB, Kim JH, Cho ZH. High-speed spiral-scan echo planar NMR imaging. IEEE Trans. Med. Imaging, 1986; 5: 2–7.
8. Meyer CH, Hu BS, Nishimura DG, Macovski A. Fast spiral coronary artery imaging. Magn. Reson. Med. 1992; 28: 202–213.
9. Hennig J, Nauerth A, Friedburg H. RARE imaging. A fast imaging method for clinical MRI. Magn. Reson. Med. 1986; 3: 823–833.
10. Frahm J, Haase A, Matthaei D, Merboldt KD, Hänicke W. Rapid NMR imaging using stimulated echoes. J. Magn. Reson. 1985; 65: 130–135.
11. Rasche V, de Boer RW, Holz D, Proksa R. Continuous radial data acquisition for dynamic MRI. Magn. Reson. Med. 1995; 34: 754–761.
12. Zhang S, Block KT, Frahm J. Magnetic resonance imaging in real time: advances using radial FLASH. J. Magn. Reson. Imaging, 2010; 31: 101–109.
13. Riederer SJ, Tasciyan T, Farzaneh F, Lee JN, Wright RC, Herfkens RJ. MR fluoroscopy: technical feasibility. Magn. Reson. Med. 1988; 8: 1–15.
14. Uecker M, Hohage T, Block KT, Frahm J. Image reconstruction by regularized nonlinear inversion – joint estimation of coil sensitivities and image content. Magn. Reson. Med. 2008; 60: 674–682.
15. Uecker M, Zhang S, Frahm J. Nonlinear inverse reconstruction for real-time MRI of the human heart using undersampled radial FLASH. Magn. Reson. Med. 2010; 63: 1456–1462.
16. Block KT, Uecker M, Frahm J. Undersampled radial MRI with multiple coils. Iterative image reconstruction using a total variation constraint. Magn. Reson. Med. 2007; 57: 1086–1098.
17. O'Sullivan JD. A fast sinc function gridding algorithm for Fourier inversion in computer tomography. IEEE Trans. Med. Imaging, 1985; 4: 200–207.
18. Kaiser JF. Nonrecursive digital filter design using the I_0-SINH window function. *Proceedings of the IEEE International Symposium on Circuits and Systems* San Francisco, CA, USA, 1974; 20–23.
19. Jackson JI, Meyer CG, Nishimura DG. Selection of a convolution function for Fourier inversion using gridding. IEEE Trans. Med. Imaging, 1991; 10: 473–478.
20. Sodickson DK, Manning WJ. Simultaneous acquisition of spatial harmonics (SMASH): fast imaging with radiofrequency coil arrays. Magn. Reson. Med. 1997; 38: 591–603.
21. Pruessmann KP, Weiger M, Scheidegger MB, Boesiger P. SENSE: sensitivity encoding for fast MRI. Magn. Reson. Med. 1999; 42: 952–962.
22. Bakushinsky AB, Kokurin MYu. *Iterative Methods for Approximate Solution of Inverse Problems*. Springer: Dordrecht, 2004.
23. Wajer F, Pruessmann KP. Major speedup of reconstruction for sensitivity encoding with arbitrary trajectories. *Proceedings of the 9th Annual Meeting ISMRM* Glasgow, UK 2001; 767.
24. Buehrer M, Pruessmann KP, Boesiger P, Kozerke S. Array compression for MRI with large coil arrays. Magn. Reson. Med. 2007; 57: 1131–1139.
25. Tukey JW. *Exploratory Data Analysis*. Addison-Wesley: Reading, MA, 1977.
26. Lustig M, Donoho D, Pauly JM. Sparse MRI: the application of compressed sensing for rapid MR imaging. Magn. Reson. Med. 2007; 58: 1182–1195.
27. Mistretta CA, Wieben O, Velikina J, Block W, Perry J, Wu Y, Johnson K, Wu Y. Highly constrained backprojection for time-resolved MRI. Magn. Reson. Med. 2006; 55: 30–40.
28. Madore B, Glover GH, Pelc NJ. Unaliasing by Fourier-encoding the overlaps using the temporal dimension (UNFOLD), applied to cardiac imaging and fMRI. Magn. Reson. Med. 1999; 42: 813–828.
29. Kellman P, Epstein FH, McVeigh ER. Adaptive sensitivity encoding incorporating temporal filtering (TSENSE). Magn. Reson. Med. 2001; 45: 846–852.

